metals

Article

Study on Constructing Indoor Accelerated Simulation Methods for Steel with Galvalume Coating Exposed to Marine Atmosphere

Luntao Wang, Hongkai Wang, Bo Li, Hao Yu, Hao Zhang, Junhang Chen, Chenghui Yin and Kui Xiao *

Institute for Advanced Materials and Technology, University of Science and Technology Beijing, Beijing 100083, China
* Correspondence: xiaokui@ustb.edu.cn

Abstract

To investigate the corrosion behavior and mechanism of steel with galvalume coating (Zn–55%Al–1.6%Si) in marine atmospheric environments, an indoor accelerated corrosion test method was constructed. Both marine atmospheric exposure tests and spectrum-based accelerated corrosion tests were carried out to compare the corrosion kinetics, corrosion products, and electrochemical behavior. A corrosion prediction model was established using the weight-loss method. Surface morphologies were observed by scanning electron microscopy (SEM), the compositions of corrosion products were identified by X-ray diffraction (XRD), and electrochemical tests were conducted to elucidate the time-dependent electrochemical characteristics. The results showed that after two years of natural exposure and 16 cycles of accelerated testing, the specimens exhibited mainly uniform corrosion of the galvalume coating without significant localized corrosion. The corrosion products were primarily composed of ZnO, $Zn_5(OH)_6(CO_3)_2$, $Zn_5(OH)_8Cl_2{\cdot}H_2O$, and Al_2O_3. The corrosion potential increased while the corrosion current density decreased with prolonged testing, indicating that the corrosion product film effectively inhibited corrosion and enhanced protection. By integrating the corrosion kinetics, product composition, and electrochemical mechanism from both outdoor and indoor tests, the constructed spectrum-based accelerated test method demonstrated good correlation with actual marine atmospheric corrosion processes, providing a reliable approach for evaluating the corrosion resistance and service life of steel with galvalume coating in marine environments.

Keywords: galvalume coating steel; marine atmospheric environment; accelerated corrosion simulation method; corrosion prediction model; correlation

check for updates

Academic Editor: Petros E. Tsakiridis

Received: 17 September 2025
Revised: 4 October 2025
Accepted: 10 October 2025
Published: 14 October 2025

Citation: Wang, L.; Wang, H.; Li, B.; Yu, H.; Zhang, H.; Chen, J.; Yin, C.; Xiao, K. Study on Constructing Indoor Accelerated Simulation Methods for Steel with Galvalume Coating Exposed to Marine Atmosphere. *Metals* **2025**, *15*, 1143. https://doi.org/10.3390/met15101143

Copyright: © 2025 by the authors. Licensee MDPI, Basel, Switzerland. This article is an open access article distributed under the terms and conditions of the Creative Commons Attribution (CC BY) license (https://creativecommons.org/licenses/by/4.0/).

1. Introduction

Zn–Al alloy-based coating systems, owing to their outstanding overall protective performance, are regarded as highly promising solutions for corrosion protection of power transmission and transformation equipment. These coatings are typically fabricated by galvalume coating galvanizing or thermal spraying. A representative example is the Galvalume coating with a composition of 55% Al, 43.5% Zn, and 1.6% Si [1]. The coating exhibits a characteristic dual-phase dendritic microstructure in which the Al-rich dendrites provide barrier protection, while the Zn-rich network acts as sacrificial anodes, and their synergistic effect significantly enhances corrosion resistance [2,3]. At the substrate–coating interface, the formation of Fe–Al–Zn intermetallic layers such as $Fe_2Al_5Zn_x$ effectively suppresses

interfacial diffusion and coating degradation [4,5]. Numerous studies have demonstrated that the service life of Zn–Al alloy coatings in various atmospheric environments can be two to six times longer than that of conventional galvanized coatings [6–8].

The addition of aluminum in Zn–Al coatings significantly enhance their chemical stability. During the corrosion process, the electrochemical behavior and the evolution of the corrosion product layer directly determine the service life of the coating. The Zn-rich phase preferentially corrodes as sacrificial anodes, while the Al-rich phase forms dense Al_2O_3 or $Al(OH)_3$ passive films [9,10]. It has been demonstrated that the presence of Al-rich dendritic regions is the key factor for the excellent long-term atmospheric corrosion resistance of these coatings [3].

The incorporation of aluminum not only modifies the properties of the coating melt and its reaction with the steel substrate but also promotes the formation of Fe–Al–Zn intermetallic compound layers, such as $Fe_2Al_5Zn_x$. These dense layers effectively inhibit the severe interdiffusion between the steel substrate and zinc, thereby controlling coating brittleness, improving adhesion, and delaying premature degradation [11]. In addition, aluminum refines the solidified microstructure of the coating. During long-term exposure, the corrosion products of aluminum interact with those of zinc to form more stable and compact composite corrosion products, such as Zn/Al-layered double hydroxide [12]. These corrosion products fill surface pores and defects of the coating, exhibit excellent ion-exchange and barrier properties, significantly reduce the corrosion rate, and impart a certain degree of self-healing capability to the coating [8].

In sulfur-containing environments, aluminum can further form basic aluminum sulfates, enhancing the protective effect [13]. In acidic environments (pH = 3–5), Zn preferentially dissolves, followed by film formation by the Al phase, and the stability of the product layer strongly depends on both the environmental pH and ionic composition [14,15]. It should be emphasized that the addition of aluminum does not completely replace the cathodic protection provided by zinc but rather establishes a synergistic mechanism. When the coating is scratched or damaged, the exposed Zn-rich phase still serves as sacrificial anodes, providing effective cathodic protection for the steel substrate [16,17]. This dual mechanism of "active protection combined with passive barrier protection" ensures that the coating maintains excellent protective performance throughout different stages of exposure.

Despite the excellent performance of Zn–Al alloy coatings and continuous improvements in accelerated test methods, the vast majority of standardized laboratory tests, such as ISO 9227 NSS [18] and ASTM B117 [19], still focus primarily on neutral media [20–22]. Research on their corrosion mechanisms under simulated industrial–marine polluted atmospheres, characterized by the coexistence of high concentrations of SO_2, Cl^-, and NO_x, remains limited. In acidic deposition environments, the failure mechanisms of the coatings, the stability of the product layer, and their correlation with outdoor exposure are still not well understood.

With respect to the correlation between laboratory accelerated tests and outdoor exposure, existing studies have revealed both important consistencies and discrepancies. However, the corrosion mechanisms and morphologies of corrosion products obtained from different test methods often deviate from those observed under actual atmospheric exposure. Morcillo et al. [23] reported that the real-world performance of 55%Al–Zn coatings in marine atmospheres was superior to that predicted by salt spray tests, due to the formation of more stable corrosion product films outdoors. Seré et al. [24] further highlighted that relying solely on neutral salt spray tests cannot accurately reproduce the complex effects of wet–dry cycles, ultraviolet irradiation, and the synergistic action of pollutants such as SO_2 and Cl^- present in real atmospheric environments. In recent years, cyclic tests designed to simulate specific conditions, such as Prohesion tests and acidic

salt spray tests, have been demonstrated to reproduce outdoor corrosion features more reliably. Research [25] has shown that adjusting pH, ion composition, and wet–dry cycling parameters can improve the correlation between laboratory tests and field exposures, particularly in industrial–marine mixed polluted atmospheres.

It is noteworthy that for specific application scenarios of Zn–Al alloy coatings in power transmission and transformation facilities, such as grounding grids exposed to humid saline soils or fittings subjected to alternating industrial acid rain and condensation, more targeted accelerated testing protocols are still required [26,27]. Therefore, it is necessary to employ accelerated tests with higher environmental relevance, such as cyclic acidic salt spray tests, in combination with electrochemical techniques and microstructural analyses. Such approaches can provide a systematic understanding of the corrosion kinetics, corrosion product composition, and structural evolution of Zn–Al coatings in simulated polluted marine atmospheric environments [28,29], and facilitate the establishment of correlation models with long-term outdoor exposure data. This will ultimately provide a more reliable theoretical basis and service life prediction framework for their application in power transmission and transformation projects under harsh environmental conditions.

In this study, the marine atmospheric environment was investigated with a focus on Wenchang, a typical coastal region. Atmospheric data, including temperature, relative humidity, rainfall, and pollutant concentrations, were collected and analyzed to identify the main environmental factors influencing corrosion. Based on the statistical analysis of key parameters such as relative humidity, temperature, and pollutant species, an accelerated corrosion spectrum simulating the marine atmosphere was designed using equivalent conversion factors for galvalume coating steel. Both outdoor exposure tests and indoor accelerated corrosion tests were conducted. The correlation of the simulated spectrum with actual marine atmospheric conditions was validated by weight-loss measurements, scanning electron microscopy (SEM), three-dimensional laser confocal microscopy, X-ray diffraction (XRD), and electrochemical techniques. The findings provide reference data for material selection and corrosion protection design of power transmission and transformation facilities operating in tropical marine atmospheric environments.

2. Materials and Methods

2.1. Materials

The test material selected was galvalume-coated steel sheets with a metallic coating composed of 55% Al, 43.4% Zn, and 1.6% Si. The galvalume coating, with a thickness of 0.5 mm, was produced by a continuous hot-dip process. During fabrication, the steel sheets were immersed in a molten Al–Zn–Si alloy bath at 610 °C for approximately 5 s, then withdrawn from the bath at a speed of 1.5 m/s. A pair of air knives (0.02 MPa) (XYZ-200, EXAIR Corporation, Cincinnati, OH, USA) was used to blow off excess molten alloy, salts, and oxides from the surface to ensure uniform coating thickness and good surface quality. The coated sheets were subsequently cooled to room temperature in a cooling chamber. To prevent oxidation during heating and hot-dipping, the molten alloy bath was maintained under a high-purity argon (99.999%) protective atmosphere. The relevant parameters are summarized in Table 1. The specimens were prepared in the as-coated condition using wire cutting and mechanical polishing. Since the side surfaces of the cut specimens were not covered by the metallic coating and directly exposed the steel substrate, protective measures were applied to ensure accuracy and eliminate side effects. Specifically, the specimen edges were sealed with 3 M adhesive tape, and any gaps were further filled with Kafuter glue (K-705 RTV Silicone Adhesive, Guangdong Kafuter Adhesive Co., Guangzhou, China) to prevent liquid penetration. Prior to testing, the specimen surfaces were degreased with anhydrous ethanol and then dried in a drying oven) (DHG-9140A, Shanghai Yiheng

Scientific Instrument Co., Shanghai, China), ensuring a completely clean and dry surface. For each corrosion weight-loss and electrochemical test, three replicate specimens were used, and the reported values represent the average to ensure statistical robustness.

Table 1. Galvalume coating steel related parameter.

Sample	Coating Thickness (mm)	Coating Weight (g/m^2)	Coated Steel Sheet Size (cm)
Galvalume coating steel	0.5	120	150 × 75 × 1

2.2. Outdoor Exposure Corrosion Test

Galvalume coating steel specimens were exposed at the Wenchang station in Hainan, China at a 45° angle for 1, 1.5, and 2 years, with sampling and analysis conducted after each exposure period. For each exposure duration, at least three replicate specimens were used to ensure reproducibility and statistical reliability, and the reported data represent averaged values.

Figure 1 presents the monthly variations in key atmospheric parameters recorded at the Wenchang marine exposure site, including temperature, relative humidity, chloride ion (Cl^-) and sulfate ion (SO_4^{2-}) deposition rates. The temperature remained high throughout the year, ranging from 27 to 28 °C during January–March to a peak of 35 °C in August, with an annual average of about 31 °C, reflecting a warm tropical marine climate. The relative humidity was consistently above 80%, maintaining a persistently moist atmosphere conducive to continuous electrolyte film formation on metallic surfaces. The Cl^- deposition rate increased sharply during the humid monsoon season (July–September), reaching its maximum in late summer due to enhanced sea-salt aerosol transport, while the SO_4^{2-} deposition rate showed moderate fluctuations, with higher values in spring and autumn, influenced by industrial emissions and long-range pollutant transport. Collectively, these data characterize Wenchang as a warm, humid, chloride-rich marine–industrial mixed atmosphere representative of coastal southern China.

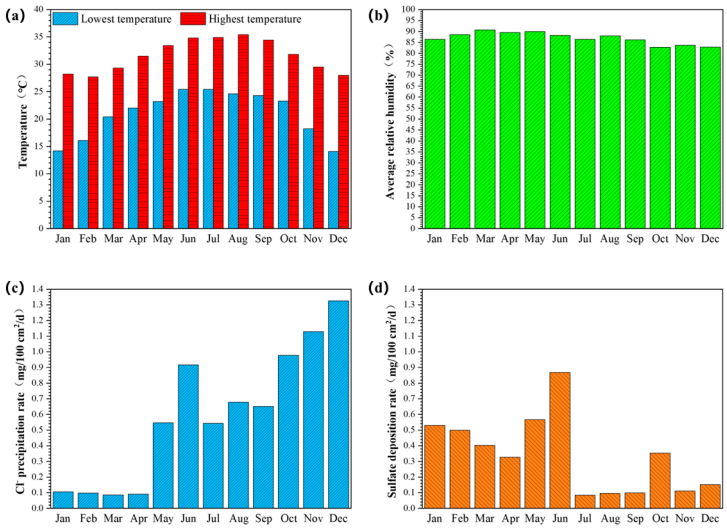

Figure 1. Monthly variation in major environmental factors at the Wenchang marine atmospheric site: (**a**) temperature (blue and red bars show the monthly average and maximum values, respectively), (**b**) relative humidity (green bars), (**c**) chloride ion (Cl^-) deposition rate (light blue bars), and (**d**) sulfate ion (SO_4^{2-}) deposition rate (orange bars).

2.3. Accelerated Corrosion Testing Method

Based on the statistical analysis of the environmental parameters, temperature, relative humidity, and Cl^-/SO_4^{2-} concentrations were identified as the dominant factors

influencing the corrosion behavior of galvalume-coated steel. These variables were therefore selected as the key inputs for constructing the accelerated corrosion spectrum. The designed test cycle consists of salt spray, drying, and humid-heat stages, which effectively reproduce the wet–dry transitions and ionic deposition characteristics typical of the natural marine atmosphere. Although the proposed test shares certain structural similarities with the traditional salt spray test, it incorporates quantitatively derived, site-specific environmental coefficients, enabling a more realistic simulation of marine corrosion processes. These coefficients were further applied to determine the number of test cycles and the specific parameters of each module in the environmental spectrum, thereby establishing a spectrum-based accelerated corrosion test method representative of marine atmospheric conditions (Figure 2).

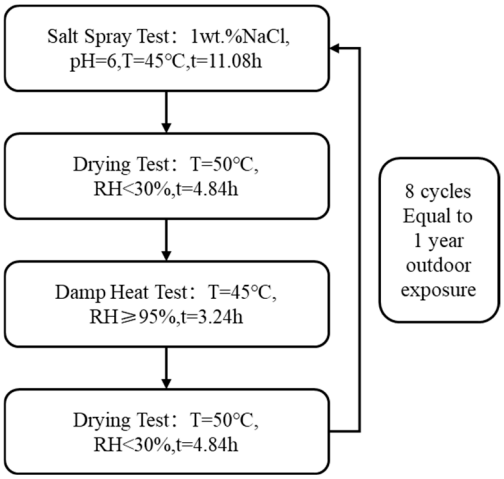

Figure 2. Accelerated test method for coastal atmospheric environment spectrum.

In the laboratory accelerated test, one complete cycle was defined as 24 h and consisted of four modules: a salt spray stage (11.08 h at 45 °C with a 1 wt.% NaCl solution, pH ≈ 6), a drying stage (4.84 h at 50 °C and RH < 30%), a humid-heat stage (3.24 h at 45 °C and RH > 95%), and a second drying stage (4.84 h at 50 °C and RH < 30%). Eight cycles corresponded to one equivalent year of exposure, and testing and analysis were performed after 1 year (8 cycle), 1.5 years (12 cycles), and 2 years (16 cycles). This equivalence was determined based on the statistical conversion of atmospheric parameters such as temperature, humidity, and pollutant deposition frequency, and was subsequently validated by comparison with the corrosion rates obtained from outdoor exposure tests. At each accelerated test point, a minimum of three replicate specimens were evaluated, and the reported data represent the averaged results to ensure reproducibility and statistical robustness.

Furthermore, the proposed spectrum-based test design conceptually aligns with international standards such as ASTM G85 [30] and ISO 20340 [31], both of which employ cyclic exposure combining salt fog, drying, and humid or wet stages to reproduce marine conditions. ASTM G85 (Annex A5) recommends a dilute electrolyte cyclic fog–dry sequence (1 h fog + 1 h dry) under controlled temperature and humidity to simulate wet–dry alternation, while ISO 20340 [31] specifies a 168 h cyclic regime integrating salt spray (25 °C, 72 h), drying (23 °C, 24 h), and UV/condensation (60 °C, 48 h) stages to replicate offshore exposure. The present spectrum-based method follows the same principle of multi-factor coupling but incorporates site-calibrated environmental coefficients derived from actual marine atmospheric data, thereby providing a more quantitative correlation between laboratory acceleration and natural exposure behavior.

2.4. Morphology of Corrosion Products

The macroscopic morphology of galvalume coating steel specimens after different cycles of indoor accelerated corrosion tests and outdoor exposure tests was recorded using a Nikon D7000 digital camera(Nikon Corporation, Tokyo, Japan). The surface micromorphology of the descaled specimens was examined with a 3D laser confocal microscope (VK-X250, Keyence Corporation, Osaka, Japan). A scanning electron microscope (SEM, Quanta 250, FEI Company, Hillsboro, OR, USA) was employed to observe the surface and cross-sectional microstructures of specimens after various exposure periods. In addition, an energy-dispersive spectroscopy (EDS) system (EDAX, Mahwah, NJ, USA) attached to the SEM was used for both point and area analyses to determine the elemental distribution and composition of the corrosion products on the surface and cross-sections.

2.5. Corrosion Kinetics

The corrosion products on the specimen surfaces were removed in accordance with GB/T 16545-2015 [32]. After each exposure, three parallel specimens were taken for corrosion mass loss measurement. The corroded samples were first lightly brushed to remove loose and bulky corrosion products. The corroded samples were lightly brushed to remove loose products then ultrasonically cleaned in a 100 g/L ammonium acetate (CH_3COONH_4) solution at 70 °C for 5–10 min, rinsed with deionized water, immersed in ethanol, and dried with warm air. The cleaned specimens were stored in a desiccator for 24 h before weighing. The initial mass (m_0) and the mass after descaling (m_1) were recorded. With the exposed surface area (S) and the exposure duration (t) measured, the corrosion rate (v) was calculated using Equation (1):

$$v = \frac{m_0 - m_1}{S \cdot t} \tag{1}$$

where v is the corrosion rate (g/(m^2·y)); m_0 is the initial mass of the specimen (g); m$_1$ is the mass after removal of corrosion products (g); S is the exposed surface area (m^2); and t is the corrosion time (y).

The thickness loss (D) was calculated according to Equation (2):

$$D = \frac{m_0 - m_1}{\rho \cdot S} \tag{2}$$

where D is the thickness loss (μm), and ρ is the density of the coating. For galvalume coating steel, ρ was taken as 7.85 g/cm^3.

2.6. Corrosion Product Analysis

Since only a small amount of corrosion products formed on the surface of the galvalume coating steel specimens, it was not possible to collect sufficient powder for X-ray diffraction (XRD) analysis. Therefore, the specimens after different exposure periods were cut into small pieces with dimensions of 10 mm × 10 mm for bulk corrosion product analysis. The surface corrosion products were analyzed using an X-ray diffractometer (D8 ADVANCE, Bruker AXS GmbH, Karlsruhe, Germany) with Cu Kα_1 radiation. The diffraction patterns were obtained over a 2θ range of 10–90° at a scanning rate of 10°/min.

2.7. Electrochemical Test

Electrochemical impedance spectroscopy (EIS) and potentiodynamic polarization tests were performed at room temperature (25 °C) using a CS3154 electrochemical workstation (KOST, Wuhan, China) on specimens after different exposure periods. A conventional three-electrode system was employed, in which the working electrode was the corroded

specimen with an exposed area of 0.785 cm^2 (a circular area with a diameter of 1 cm), the reference electrode was a saturated calomel electrode (SCE), and the counter electrode was a platinum electrode. The electrolyte was a 10.00 g/L NaCl solution, prepared using Class A volumetric glassware and an analytical balance (ME204, Mettler Toledo, Greifensee, Switzerland) (0.1 mg readability). Prior to the polarization measurements, the open circuit potential (OCP) was monitored for 1800 s to allow the system to stabilize. Potentiodynamic polarization scans were then conducted within a potential range of −0.5 V to +0.5 V versus OCP, at a scan rate of 0.5 mV/s.

3. Results

3.1. Marine Atmospheric Exposure Test

The corrosion rate was determined using the weight-loss method to obtain the corrosion mass loss rate of the specimens. Based on the measured weight loss, the thickness loss rates of galvalume coating steel after 1, 1.5, and 2 years of marine atmospheric exposure were calculated. As shown in Table 2, the thickness loss of the specimens increased progressively with longer exposure durations in the marine atmosphere.

Table 2. Corrosion mass loss of galvalume coating steel after marine atmospheric exposure.

Time/Year	1	1.5	2
Corrosion mass loss per unit area (g/m^2)	15.27	23.86	27.12
Average thickness loss (μm)	2.09	3.27	3.72
Average corrosion rate (μm/y)	2.09	2.18	1.86

As presented in Table 2, the corrosion mass loss per unit area of galvalume coating steel increased progressively with exposure duration, from 15.27 g/m^2 after 1 year to 27.12 g/m^2 after 2 years. The corresponding average thickness loss rose from 2.09 μm to 3.72 μm, demonstrating a clear cumulative degradation over time. In contrast, the average corrosion rate decreased from 2.09 μm/y in the first year to 1.86 μm/y after 2 years, indicating that the corrosion process tended to slow down with longer atmospheric exposure.

The macroscopic morphology of galvalume coating steel under marine atmospheric exposure was analyzed, and the results are shown in Figure 3. The unexposed specimen exhibited distinct spangles with a bright metallic luster and a gray-white appearance. After 1 year of exposure, the surface became noticeably darker, lost its metallic luster, and the distribution of spangles decreased, with the overall color turning gray-black. After 2 years, the surface color further darkened, the metallic luster was almost completely lost, and a few black rust spots appeared. After 2 years, the surface turned dark gray, the spangles became barely visible, and the number of black rust spots increased compared with the 1.5 years specimen, although they remained sparsely distributed.

From the macroscopic morphology of galvalume coating steel after 2 years of marine atmospheric exposure, it can be observed that the specimen surfaces had completely lost their metallic luster, with a distinct color change and darkening of the surface. However, no significant corrosion damage was detected, and the surfaces remained intact. This indicates that during the 2 years marine atmospheric exposure test, the galvalume coating Zn–Al coating provided effective protection to the steel substrate, demonstrating good corrosion resistance.

To evaluate the corrosion behavior of scratched regions, the macroscopic morphology of galvalume-coated steel with artificial scratches was examined after 1, 1.5, and 2 years of marine atmospheric exposure, and the results are presented in Figure 4. The scratches were introduced manually using a carbide scribe, approximately 10 cm in length and about 0.3 mm in width, penetrating through the Galvalume coating to the steel substrate

to simulate mechanical damage. The results show that the scratch width exhibited no significant change during the entire exposure period. After 2 years, only a small amount of white corrosion products was observed at the scratched sites. During prolonged exposure, the scratches became less visible due to the accumulation of corrosion products and surface deposits, which may obscure their appearance in macroscopic images. Throughout the tests, no reddish-brown corrosion products were detected, and the scratch width remained nearly constant. These findings suggest that protective corrosion products formed within the scratched regions during exposure, providing effective barrier protection to the substrate and preventing further corrosion propagation.

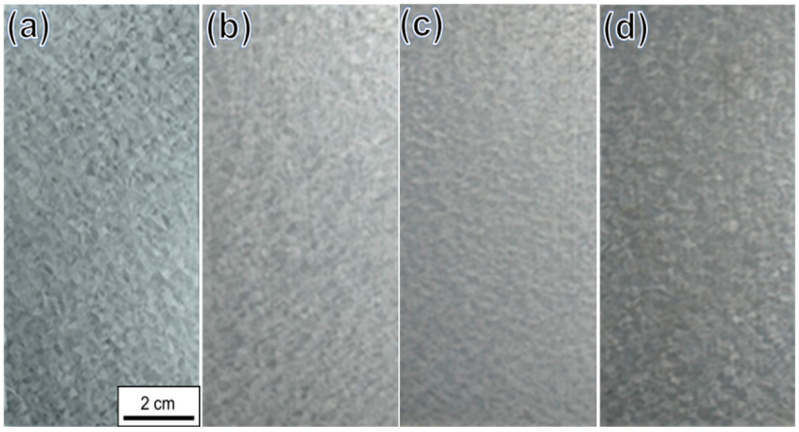

Figure 3. Macroscopic corrosion morphology of galvalume coating steel after marine atmospheric exposure: (**a**) 0 y, (**b**) 1 y, (**c**) 1.5 y and (**d**) 2 y.

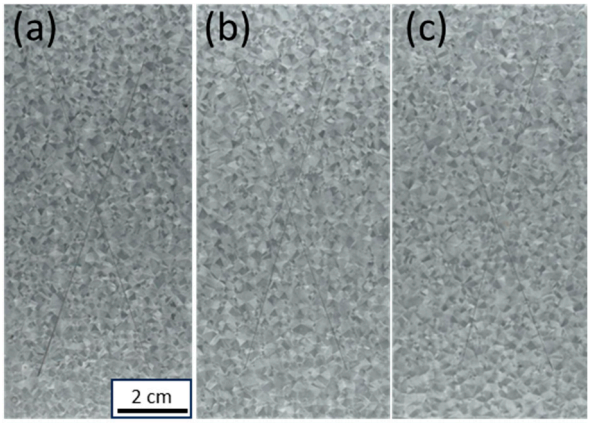

Figure 4. Macroscopic corrosion morphology of scratched galvalume coating steel after marine atmospheric exposure: (**a**) 1 y, (**b**) 1.5 y, (**c**) 2 y.

Figure 5 shows three-dimensional confocal images of galvalume coating steel after removal of corrosion products following 1, 1.5, and 2 years of marine atmospheric exposure. The results indicate that the corrosion was mainly uniform, but after 1.5 and 2 years the damage was more pronounced and the surface flatness decreased compared with that after 1 year of exposure.

Figure 6 shows the SEM surface morphology of galvalume coating steel after 1, 2, and 2.5 years of marine atmospheric exposure, while Table 3 presents the EDS results of surface elemental compositions (at%) after different exposure durations. After 1 year of exposure, the specimen surface remained relatively smooth, with corrosion preferentially occurring in the Zn-rich regions. The formation of corrosion products was first observed in these Zn-rich zones, appearing as island-like structures, and the products mainly consisted of

Al, Zn, C, O, and Cl. After 1.5 years of exposure, the number of island-like and granular corrosion products increased, and some of them aggregated to form larger corrosion clusters. These products were mainly composed of Zn, Al, C, O, and Cl. After 2 years, the surface corrosion became more pronounced, with abundant island-like products, and dense needle-like corrosion products were observed in the Zn-rich regions, which may act as a physical barrier to slow further corrosion. Elemental analysis indicated that Zn had a higher proportion than Al in the corrosion products, which can be attributed to the preferential dissolution of Zn in the Zn-rich regions, accompanied by limited Al dissolution, leading to the formation of Zn- and Al-containing corrosion products.

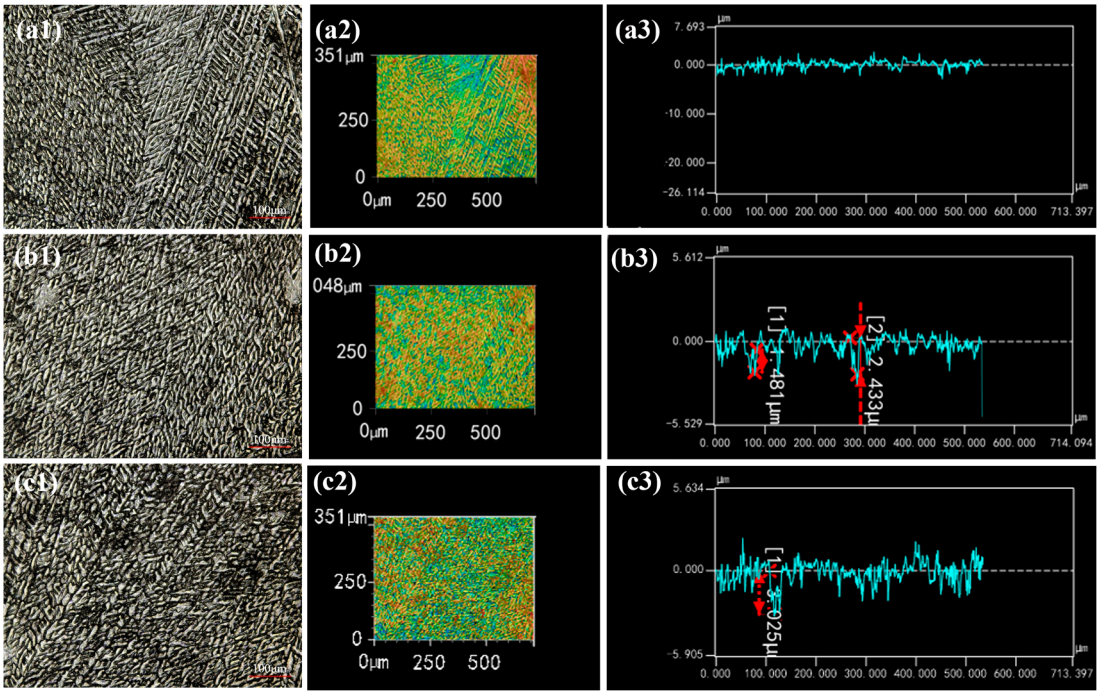

Figure 5. Three-dimensional confocal images of galvalume coating steel after removal of corrosion products following different periods of marine atmospheric exposure: (**a**) 1 y, (**b**) 1.5 y, (**c**) 2 y. (**a1**–**c1**) Surface morphology; (**a2**–**c2**) corresponding 3D surface topography maps; (**a3**–**c3**) defect depth profiles (The labels [1] and [2] indicate the sampling points selected for detailed surface topography analysis)

Table 3. EDS surface elemental compositions (at%) of galvalume coating steel after different durations of marine atmospheric exposure.

Sample	O	Cl	C	Zn	Al
1 y	38.22	1.17	35.27	19.24	6.11
1.5 y	9.33	6.43	48.05	23.15	13.04
2 y	32.79	11.48	18.25	34.50	2.98

Figure 7 presents the cross-sectional corrosion morphology and elemental mapping of galvalume coating steel after 2 years of marine atmospheric exposure. The results show that O and Cl were enriched in the Zn-rich regions and at the outer surface of the coating but did not significantly penetrate into the substrate or accumulate in the steel matrix. This indicates that the Zn-rich regions corroded preferentially, while the surface corrosion products partially hindered the ingress of aggressive ions, thereby ensuring that the coating maintained good corrosion resistance during long-term exposure.

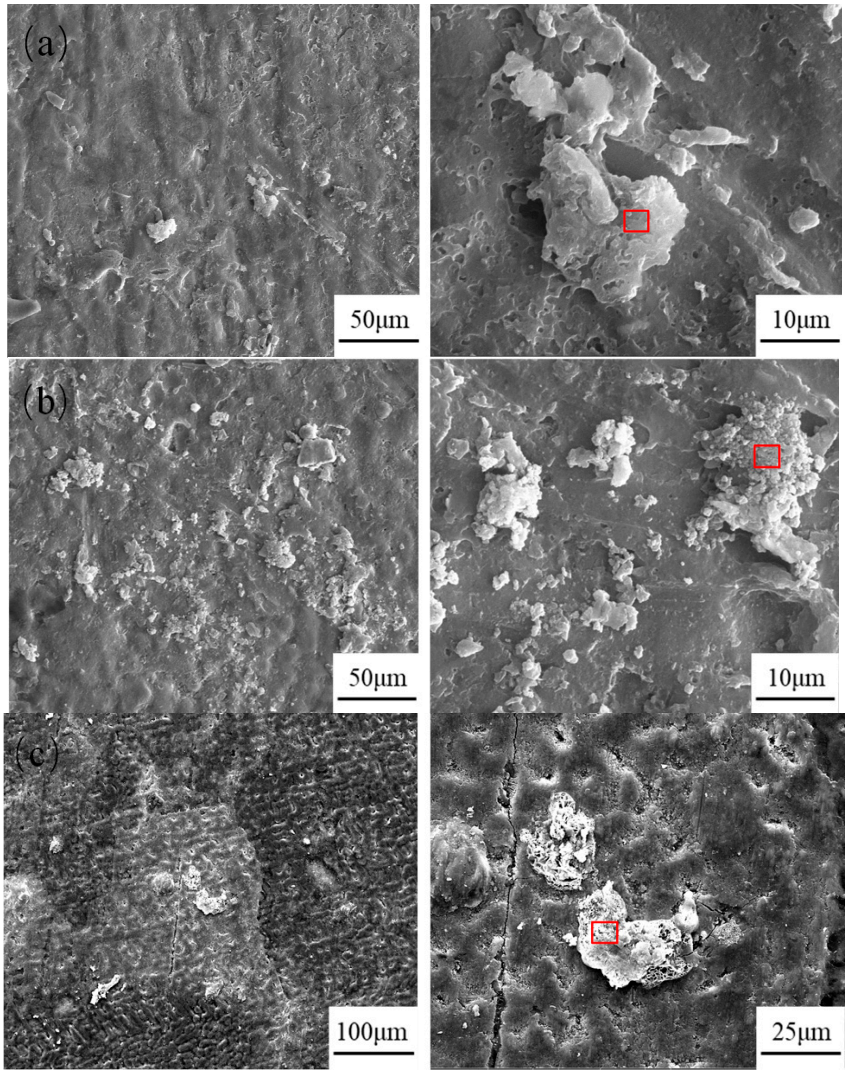

Figure 6. SEM surface morphology of galvalume coating steel after different durations of marine atmospheric exposure: (**a**) 1 y, (**b**) 1.5 y, (**c**) 2 y. (The red boxes indicate the regions selected for EDS elemental analysis).

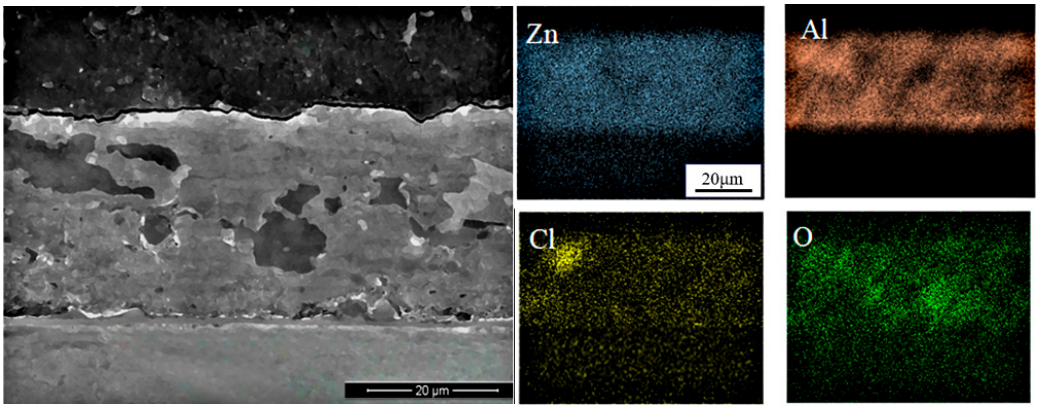

Figure 7. Cross-sectional corrosion morphology (**left**) and elemental mapping (**right**) of galvalume coating steel after 2 years of marine atmospheric exposure.

Figure 8 shows the XRD patterns of corrosion products formed on galvalume coating steel after 1.5 and 2 years of marine atmospheric exposure. The results indicate that the corrosion products were mainly composed of ZnO, $Zn_5(OH)_6(CO_3)_2$, $Zn_5(OH)_8Cl_2{\cdot}H_2O$,

and Al_2O_3. Throughout the exposure period, the types of corrosion products remained similar, although their relative amounts varied. ZnO was the dominant phase, while the denser products, including $Zn_5(OH)_6(CO_3)_2$, $Zn_5(OH)_8Cl_2{\cdot}H_2O$, and Al_2O_3, covered the corroded regions and acted as barriers to the further ingress of aggressive ions. In addition, the compact white corrosion products observed on the surface may also contain Zn–Al layered double hydroxide (LDH) phases, which are known to form on Al-containing zinc coatings exposed to humid chloride environments. Such LDH-type compounds can intercalate carbonate or chloride anions and exhibit self-healing or re-passivation functions by trapping aggressive ions and regenerating hydroxide layers at local defects [33,34]. The possible presence of these Zn–Al LDH-like structures, together with ZnO and Al_2O_3 phases, contributes to the enhanced compactness and protective efficiency of the corrosion film, explaining the stable surface morphology and improved corrosion resistance observed during prolonged marine atmospheric exposure.

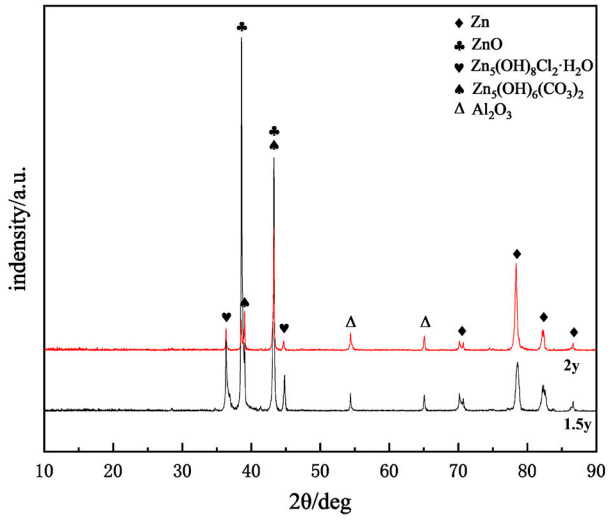

Figure 8. XRD patterns of corrosion products formed on galvalume coating steel after 1.5 and 2 years of marine atmospheric exposure.

Figure 9 and Table 4 present the potentiodynamic polarization curves and fitted data of galvalume coating steel after 1, 1.5, and 2 years of marine atmospheric exposure. As shown in the polarization curves, the corrosion process was mainly controlled by the cathodic reaction, which was dominated by either hydrogen evolution or oxygen reduction, while the anodic reaction corresponded to metal dissolution. According to Table 4, the corrosion potential increased with exposure time, whereas the corrosion current density continuously decreased. This indicates that the corrosion products formed on the surface effectively hindered further corrosion, thereby enhancing the protective performance of the coating.

The fitted potentioldynamic data in Table 4 also demonstrate that galvalume coating steel exhibited good corrosion resistance, with the corrosion products forming a denser structure that covered the corroded regions and reduced the corrosion current density. SEM observations confirmed that corrosion products preferentially formed in the Zn-rich regions and subsequently covered the corroded sites. At later stages of exposure, needle-like corrosion products developed in these Zn-rich areas, providing a more compact barrier and further reducing the corrosion rate. In addition, XRD analysis revealed the presence of Al_2O_3 together with higher amounts of $Zn_5(OH)_6(CO_3)_2$ and $Zn_5(OH)_8Cl_2{\cdot}H_2O$, which contributed to blocking the ingress of corrosive species and thus significantly decreased the overall corrosion rate.

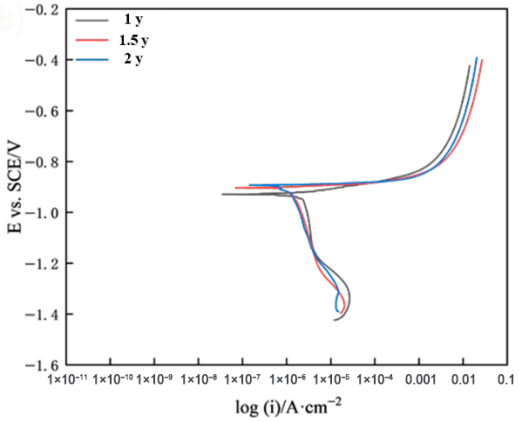

Figure 9. Potentiodynamic polarization curves of galvalume coating steel after 1, 1.5, and 2 years of outdoor atmospheric exposure.

Table 4. Fitted potentiodynamic polarization data of galvalume coating steel after different durations of marine atmospheric exposure.

Exposure Time	**1 y**		**1.5 y**		**2 y**	
Fitted data	V_{corr}/mV −927	i_{corr}/μA 2.378	V_{corr}/mV −905	i_{corr}/μA 1.353	V_{corr}/mV −892	i_{corr}/μA 1.146

3.2. Accelerated Corrosion Test

Accelerated corrosion tests were conducted on galvalume coating steel. The corrosion mass loss rate of the specimens was determined using the weight-loss method, and the corresponding thickness loss was then calculated from the measured weight loss, as summarized in Table 5.

Table 5. Weight-loss data of galvalume coating steel after accelerated corrosion tests simulating a marine atmospheric environment.

Cycles	**8**	**12**	**16**
Corrosion mass loss per unit area (g/m^2)	19.30	24.44	28.73
Average thickness loss (μm)	2.65	3.35	3.94
Average corrosion rate (μm/y)	2.65	2.23	1.97

Figure 10 shows the macroscopic corrosion morphology of galvalume coating steel after 8, 12, and 16 cycles of marine atmospheric spectrum-based accelerated corrosion tests. Before the test, the coating exhibited a uniform distribution of visible zinc spangles with a distinct metallic luster, and the surface appeared silver-gray. After 8 cycles, the surface became darker and the metallic luster weakened, although the zinc spangles remained clearly visible and evenly distributed. After 12 and 16 cycles, the surface color further darkened, the metallic luster was noticeably lost, and the zinc spangles became less distinct. The number of black spot-like corrosion products increased compared to that observed after 8 cycles, and their distribution remained non-uniform.

Figure 11 shows the macroscopic corrosion morphology of scratched galvalume coating steel after 8, 12, and 16 cycles of marine atmospheric spectrum-based accelerated corrosion tests. As observed, the scratches exhibited no significant changes throughout the exposure, and the scratch width remained essentially unchanged after all test cycles.

Figure 12 shows the three-dimensional confocal images of galvalume coating steel after removal of corrosion products during 8, 12, and 16 cycles of marine atmospheric spectrum-based accelerated corrosion tests. The results indicate that uniform corrosion

was the dominant form throughout the test, and no obvious corrosion pits were observed on the specimen surfaces.

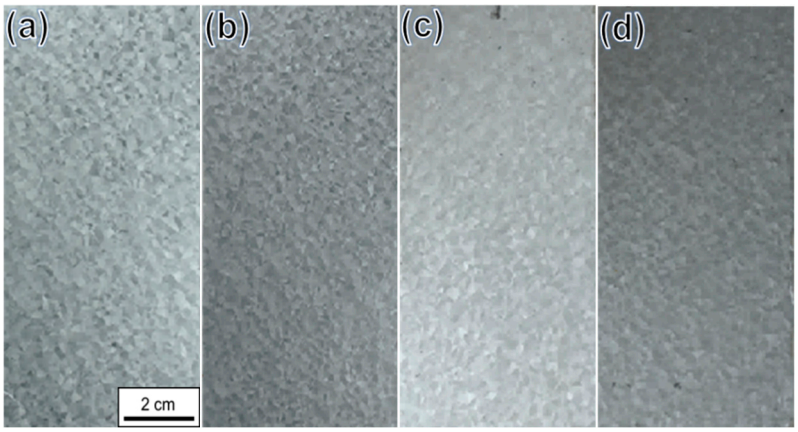

Figure 10. Macroscopic corrosion morphology of galvalume coating steel during marine atmospheric spectrum-based accelerated corrosion tests: (**a**) 0 cycle, (**b**) 8 cycles, (**c**) 12 cycles, and (**d**) 16 cycles.

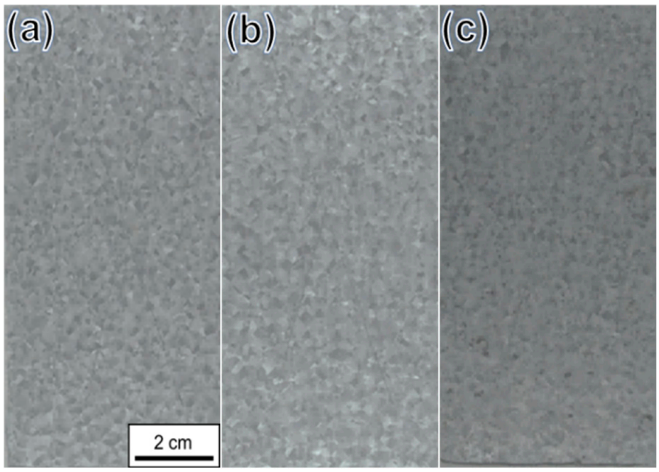

Figure 11. Macroscopic corrosion morphology of scratched galvalume coating steel during marine atmospheric spectrum-based accelerated corrosion tests: (**a**) 8 cycles, (**b**) 12 cycles, (**c**) 16 cycles.

Figure 13 shows the surface micro-morphology of galvalume coating steel after 8, 12, and 16 cycles of marine atmospheric spectrum-based accelerated corrosion tests, and Table 6 presents the surface elemental compositions of the corrosion products (at%) obtained after different exposure cycles. The surface corrosion products were examined by SEM and analyzed by EDS.

As shown in Figure 13 and Table 6, after 8 cycles, both the volume and the number of island-like corrosion products were observed, with some aggregating into larger corrosion clusters. The corrosion products at this stage mainly consisted of C, O, Cl, Zn, and Al. After 12 cycles, corrosion became more severe, and localized regions of dense, spherical corrosion products appeared, composed primarily of the same elements. By 16 cycles, corrosion was more pronounced than at 12 cycles, and compact, needle-like corrosion products had formed on the surface. These products were again mainly composed of C, O, Cl, Zn, and Al, but with Al content exceeding that of Zn, indicating that after preferential consumption of Zn-rich regions, corrosion progressed into the Al-rich regions.

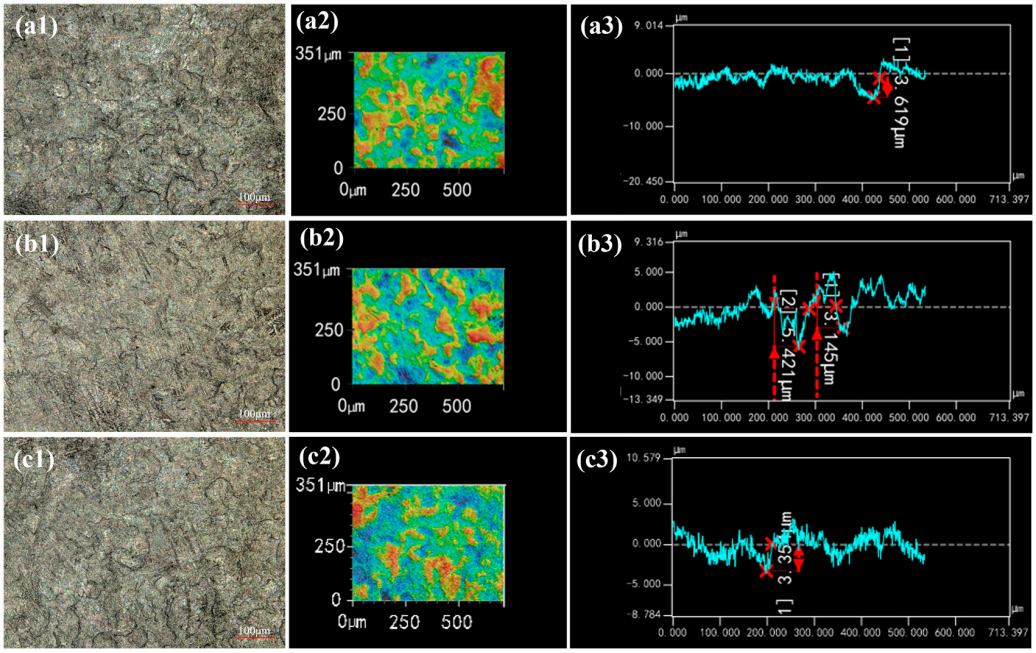

Figure 12. Three-dimensional confocal images of galvalume coating steel after removal of corrosion products during marine atmospheric spectrum-based accelerated corrosion tests: (**a**) 8 cycles, (**b**) 12 cycles, (**c**) 16 cycles. (**a1**–**c1**) Surface morphology; (**a2**–**c2**) corresponding 3D surface topography maps; (**a3**–**c3**) defect depth profiles.

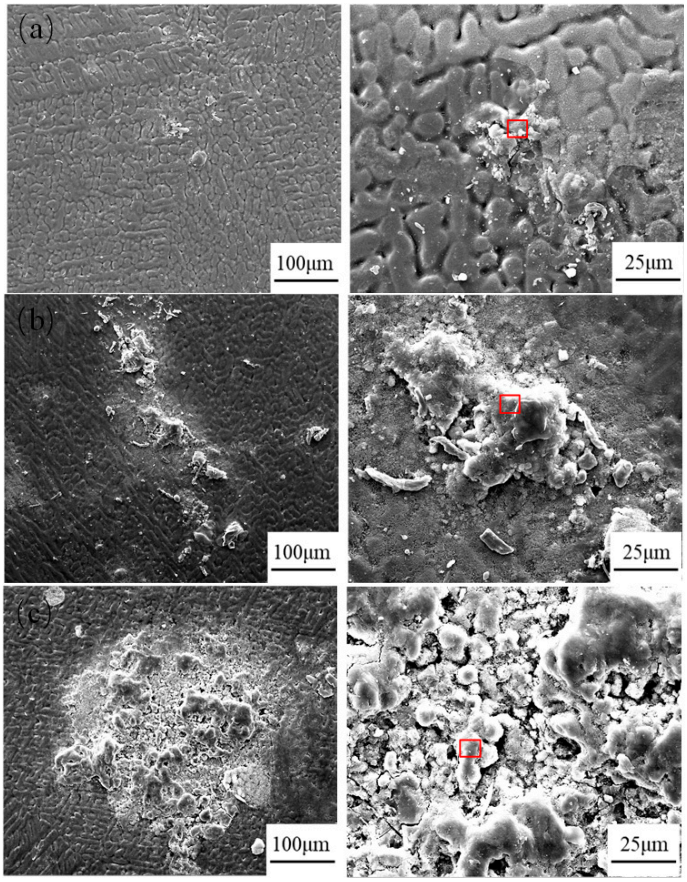

Figure 13. SEM of galvalume coating steel after different cycles of marine atmospheric spectrum-based accelerated corrosion tests: (**a**) 8 cycles, (**b**) 12 cycles, (**c**) 16 cycles. (The red boxes indicate the regions selected for EDS elemental analysis).

Table 6. EDS surface elemental compositions (at%) of corrosion products on galvalume coating steel after different cycles of marine atmospheric spectrum-based accelerated corrosion tests.

Experimental Cycles	O	Cl	C	Zn	Al
8	40.71	0.48	18.06	25.92	14.83
12	43.68	0.32	19.91	20.92	15.18
16	15.30	0.42	13.07	14.46	56.75

Figure 14 shows the XRD patterns of corrosion products formed on galvalume coating steel after 12 and 16 cycles of marine atmospheric spectrum-based accelerated corrosion tests. The results indicate that the corrosion products were mainly composed of ZnO, $Zn_5(OH)_6(CO_3)_2$, $Zn_5(OH)_8Cl_2{\cdot}H_2O$, and Al_2O_3. Among these, ZnO was the most abundant phase and provided a certain degree of protection. The denser phases, including $Zn_5(OH)_6(CO_3)_2$, $Zn_5(OH)_8Cl_2{\cdot}H_2O$, and Al_2O_3, were more prevalent in galvalume coating steel than in galvanized steel, covering the corroded regions and effectively hindering the further ingress of aggressive ions.

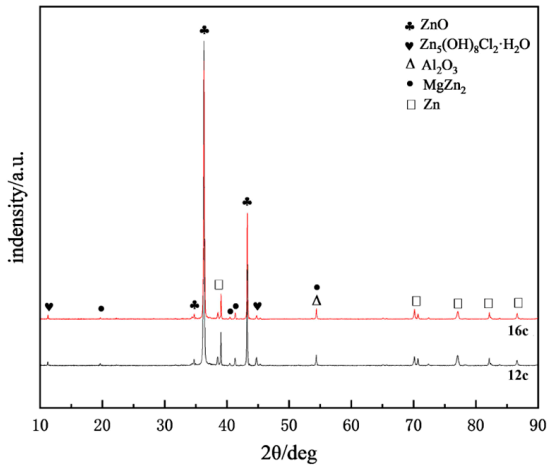

Figure 14. XRD patterns of corrosion products on galvalume coating steel after marine atmospheric spectrum-based accelerated corrosion tests.

Figure 15 and Table 7 present the potentiodynamic polarization curves and fitted results of galvalume coating steel after 0, 8, 12, and 16 cycles of marine atmospheric spectrum-based accelerated corrosion tests. The polarization curves indicate that the corrosion process was also controlled by the cathodic reaction. As shown in Table 7, the corrosion potential of galvalume coating steel increased continuously with longer exposure time, while the corrosion current density decreased. This suggests that the corrosion products formed on the coating surface effectively hindered further corrosion, thereby enhancing the corrosion resistance of the material [35]. Moreover, at the same test cycle, the corrosion potential of galvalume coating steel was lower than that of galvanized steel.

Table 7. Fitted potentiodynamic polarization data of galvalume coating steel after different cycles of marine atmospheric spectrum-based accelerated corrosion tests.

Experimental Cycles	0		8		12		16	
Fitted data	V_{corr}/mV	i_{corr}/μA	V_{corr}/mV	i_{corr}/μA	V_{corr}/mV	i_{corr}/μA	V_{corr}/mV	i_{corr}/μA
	−969	2.827	−936	2.132	−911	1.696	−904	1.332

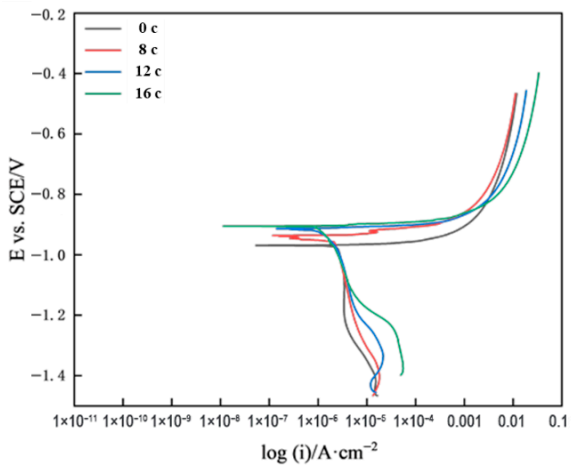

Figure 15. Potentiodynamic polarization curves of galvalume coating steel after different cycles of marine atmospheric spectrum-based accelerated corrosion tests.

3.3. Correlation Analysis Between Indoor Accelerated Tests and Outdoor Exposure Tests

The variation in thickness loss of galvalume coating steel under equivalent exposure durations in indoor and outdoor tests is shown. It can be observed that, except for the larger deviation between 1 year of marine atmospheric exposure and 1 cycle (equivalent year) of the spectrum-based accelerated test, the results were generally consistent. The deviation in the early stage indicates the influence of fluctuating outdoor environmental conditions, which led to certain discrepancies in atmospheric corrosion during the initial exposure period. However, with longer test durations, the deviations at 1.5 and 2 years decreased, and the corrosion kinetics obtained from indoor and outdoor tests exhibited good consistency.

To further quantify the correlation between indoor accelerated and outdoor exposure results, the grey relational analysis (GRA) method was applied. GRA evaluates the degree of association between data sequences based on the similarity of their developmental trends and is particularly suitable for systems with limited, uncertain, or incomplete data. Compared with conventional statistical approaches such as Pearson correlation or regression models, which typically require large datasets and assume linear relationships, GRA provides a more flexible and reliable means of correlation assessment under the constrained data conditions often encountered in corrosion studies. This method, originally proposed by Deng (1982) [36], has since been widely applied in corrosion science [37–39]. Among various grey analysis techniques, Deng's grey relational approach was adopted in this study to analyze the consistency of corrosion behavior between the accelerated and natural exposure tests. The grey relational degree (γ) was introduced to describe the correlation between the two variables.

$$Y_{0\mathrm{i}} = \frac{1}{\mathrm{n}}\sum_{k=1}^{\mathrm{n}} \xi_{0\mathrm{i}}(k) \tag{3}$$

$$\xi_{0i}(k) = \frac{\min\limits_{i}\min\limits_{k}|Y_0(k) - Y_i(k)| + \rho\max\limits_{i}\max\limits_{k}|Y_0(k) - Y_i(k)|}{|Y_0(k) - Y_i(k)| + \rho\max\limits_{i}\max\limits_{k}|Y_0(k) - Y_i(k)|} \tag{4}$$

$$Y_0(k) = \left\{ \begin{array}{c} X_0(k) \\ X_0(1) \end{array} \right\} = \{Y_0(1), Y_0(2), Y_0(3), \ldots, Y_0(n)\} \tag{5}$$

$$Y_i(k) = \left\{ \begin{array}{c} X_i(k) \\ X_i(1) \end{array} \right\} = \{Y_i(1), Y_i(2), Y_i(3), \ldots, Y_i(n)\} \tag{6}$$

$$\Delta_{0i}(k) = |Y_0(k) - Y_i(k)| \tag{7}$$

where $\max_i \max_k = |Y_0(k) - Y_i(k)|$ and $\min_i \min_k = |Y_0(k) - Y_i(k)|$ represent the maximum and minimum differences between two sequences, respectively. The resolution coefficient ρ is within the range $0 < \rho < 1$ and is typically taken as 0.5. A larger value of the grey relational degree γ_{0i} indicates a stronger correlation. In general, when $\gamma_{0i} > 0.6$, the correlation between the sequences can be considered good.

(1) Reference sequence and comparison sequence

The weight-loss data of galvalume coating steel from outdoor atmospheric exposure tests were taken as the reference sequence $X_0(k)$, where $k = 1, 1.5, 2$. The weight-loss data from marine atmospheric spectrum-based accelerated tests were taken as the comparison sequence $X_i(k)$, where $k = 1, 1.5, 2$. By performing kinetic fitting on both indoor and outdoor weight-loss data, the corresponding values at equivalent exposure times were obtained, as summarized in Table 8.

Table 8. Corrosion weight-loss data of galvalume coating steel from indoor accelerated tests and outdoor marine atmospheric exposure tests.

Experiment Time	Galvalume Coating Steel	
	Outdoor Exposure X_0	Indoor Accelerated Test X_i
1 y/8 cycles	4.02	4.33
1.5 y/12 cycles	5.56	5.48
2 y/16 cycles	6.98	6.44

(2) Initialization of corrosion weight-loss data

According to Equations (5) and (6), the corrosion weight-loss data of galvalume coating steel were initialized, as shown in Table 9.

Table 9. Initialized corrosion weight-loss data of galvalume coating steel from indoor accelerated tests and outdoor marine atmospheric exposure tests.

Experiment Time	Galvalume Coating Steel	
	Outdoor Exposure X_0	Indoor Accelerated Test X_i
1 y/8 cycles	1.74026	1.72510
1.5 y/12 cycles	2.406926	2.183267
2 y/16 cycles	3.021645	2.565737

(3) Absolute difference sequence

According to Equation (7), the initialized corrosion weight-loss data were processed to obtain the absolute difference sequence of corrosion weight-loss data, as shown in Table 10.

Table 10. Absolute difference sequence of corrosion weight-loss data for galvalume coating steel from indoor accelerated tests and outdoor marine atmospheric exposure tests.

Experiment Time	Galvalume Coating Steel
	D_2
1 y/8 cycles	0.015160
1.5 y/12 cycles	0.223659
2 y/16 cycles	0.455908

(4) Grey relational degree calculation between indoor and outdoor marine atmospheric tests

According to Equations (4) and (5), the grey relational degrees between the outdoor marine atmospheric exposure test and the spectrum-based accelerated test were calculated. As shown in Table 11, the grey relational degrees of galvalume coating steel in both outdoor exposure and accelerated tests were all greater than 0.6, indicating that the designed spectrum-based accelerated corrosion test for the marine atmospheric environment exhibited good correlation with outdoor exposure results.

Table 11. Grey relational degrees of galvalume coating steel from outdoor marine atmospheric exposure tests and spectrum-based indoor accelerated tests.

Materials	Accelerated Testing
Galvalume coating Galvalume Steel	0.6789

A comparative study of galvalume coating steel in marine atmospheric exposure and spectrum-based accelerated tests demonstrated good consistency in both corrosion products and electrochemical behavior. In both environments, dense needle-like or granular corrosion products were formed at later stages, with compositions dominated by ZnO, $Zn_5(OH)_6(CO_3)_2$, $Zn_5(OH)_8Cl_2{\cdot}H_2O$, and Al_2O_3, showing strong similarity between indoor and outdoor results. The polarization curves also exhibited comparable characteristics, with corrosion mainly controlled by cathodic reactions and anodic dissolution of Zn and Al. Moreover, in both test conditions, corrosion current density decreased while corrosion potential increased with longer exposure time, indicating progressive improvement in corrosion resistance. Overall, the results confirm that the electrochemical mechanism and corrosion evolution in accelerated tests are closely correlated with those in outdoor marine atmospheric exposure.

4. Conclusions

In this study, the corrosion behavior and mechanism of galvalume coating steel under indoor accelerated tests and outdoor marine atmospheric exposure were comparatively analyzed based on corrosion kinetics, corrosion products, and electrochemical responses.

(1) Throughout the entire test period, no significant corrosion products were observed on the surface, while needle-like products appeared in localized areas during the later stages. The main corrosion products were identified as ZnO, $Zn_5(OH)_6(CO_3)_2$, $Zn_5(OH)_8Cl_2{\cdot}H_2O$, and Al_2O_3. Among them, ZnO was the most abundant phase and provided partial protection, whereas $Zn_5(OH)_8Cl_2{\cdot}H_2O$ and Al_2O_3 exhibited higher density, covering the corroded regions and hindering the ingress of aggressive ions.

(2) The corrosion kinetics of galvalume coating steel in both marine atmospheric exposure and spectrum-based accelerated tests were consistent. In addition, the potentiodynamic polarization curves showed similar features under both conditions, with the corrosion process mainly controlled by cathodic reactions, and the trends of corrosion potential and corrosion current being consistent.

(3) The corrosion kinetics and electrochemical mechanisms exhibited strong consistency between the indoor accelerated and outdoor exposure tests. The types of corrosion products were also the same, with aggressive ions enriched within the coating rather than penetrating into the substrate, indicating that the Zn–Al coating effectively acted as a barrier. Grey relational analysis further showed correlation coefficients greater than 0.6, confirming that the accelerated spectrum was well designed and that the indoor accelerated corrosion tests exhibited good correlation with outdoor exposure.

Author Contributions: L.W.: Conceptualization; software; writing—original draft preparation; project administration; H.W.: methodology; visualization; B.L.: Data curation; Formal analysis; Visualization; Software; H.Y.: Conceptualization; Methodology; Investigation; Data curation; Formal analysis; H.Z.: Investigation; Validation; Formal analysis; Data curation; J.C.: Formal analysis; Data interpretation; Visualization; Methodology; C.Y.: Data curation; Resources; Visualization; Investigation; K.X.: Conceptualization; resources; data curation; writing—review and editing; supervision; funding acquisition. All authors have read and agreed to the published version of the manuscript.

Funding: This research was funded by National Key R&D Program of China (Grant No. 2024YFF0728900). This work was also supported by the Interdisciplinary Research Project for Young Teachers of USTB (Fundamental Research Funds for the Central Universities, No. FRF-IDRY-24-018).

Data Availability Statement: The datasets presented in this article are not readily available because the data are part of an ongoing study. Requests to access the datasets should be directed to [Corresponding author at xiaokui@ustb.edu.cn].

Conflicts of Interest: The authors declare that they have no known competing financial interests or personal relationships that could have appeared to influence the work reported in this paper. The funders had no role in the design of the study; in the collection, analyses, or interpretation of data; in the writing of the manuscript; or in the decision to publish the results.

References

1. Wang, S.; Liu, Q.; Wang, J.; Chen, N.; Chen, J.; Song, J.; Zhang, X.; Xiao, K. Study of the role of aluminium and corrosion mechanism in galvalume coating in the marine atmospheric environment. *Anti-Corros. Methods Mater.* **2024**, *71*, 286–294. [CrossRef]
2. Qiu, P.; Leygraf, C.; Wallinder, I.O. Evolution of corrosion products and metal release from Galvalume coatings on steel during short and long-term atmospheric exposures. *Mater. Chem. Phys.* **2012**, *133*, 419–428. [CrossRef]
3. Moreira, A.R.; Panossian, Z.; Camargo, P.; Moreira, M.F.; Da Silva, I.; De Carvalho, J.R. Zn/55Al coating microstructure and corrosion mechanism. *Corros. Sci.* **2006**, *48*, 564–576. [CrossRef]
4. Yan, D.; Yang, Y.; Dong, Y.; Chen, X.; Wang, L.; Zhang, J.; He, J. Phase transitions of plasma sprayed Fe–Al intermetallic coating during corrosion in molten zinc at 640 °C. *Intermetallics* **2012**, *22*, 160–165. [CrossRef]
5. Li, K.; Liu, Y.; Tu, H.; Su, X.; Wang, J. Effect of Si on the growth of Fe-Al intermetallic layer in Zn-11% Al-3% Mg coating. *Surf. Coat. Technol.* **2016**, *306*, 390–396. [CrossRef]
6. AD, V.; Panda, B. Corrosion behaviour of galvanised steel in alkaline sodium chloride solution. *Adv. Mater. Process. Technol.* **2022**, *8* (Suppl. 2), 826–840.
7. Penney, D.J.; Sullivan, J.H.; Worsley, D.A. Investigation into the effects of metallic coating thickness on the corrosion properties of Zn–Al alloy galvanising coatings. *Corros. Sci.* **2007**, *49*, 1321–1339. [CrossRef]
8. Edavan, R.P.; Kopinski, R. Corrosion resistance of painted zinc alloy coated steels. *Corros. Sci.* **2009**, *51*, 2429–2442. [CrossRef]
9. Palma, E.; Puente, J.; Morcillo, M. The atmospheric corrosion mechanism of 55% Al-Zn coating on steel. *Corros. Sci.* **1998**, *40*, 61–68. [CrossRef]
10. Kalendova, A. Mechanism of the action of zinc-powder in anticorrosive coatings. *Anti-Corros. Methods Mater.* **2002**, *49*, 173–180. [CrossRef]
11. Zapico Álvarez, D.; Bertrand, F.; Mataigne, J.-M.; Giorgi, M.-L. Nature of the inhibition layer in GA baths. *Metall. Res. Technol.* **2014**, *111*, 9–15. [CrossRef]
12. Gomes, C.; Mir, Z.; Sampaio, R.; Bastos, A.; Tedim, J.; Maia, F.; Rocha, C.; Ferreira, M. Use of ZnAl-layered double hydroxide (LDH) to extend the service life of reinforced concrete. *Materials* **2020**, *13*, 1769. [CrossRef]
13. Panossian, Z.; Mariaca, L.; Morcillo, M.; Flores, S.; Rocha, J.; Peña, J.; Herrera, F.; Corvo, F.; Sanchez, M.; Rincon, O. Steel cathodic protection afforded by zinc, aluminium and zinc/aluminium alloy coatings in the atmosphere. *Surf. Coat. Technol.* **2005**, *190*, 244–248. [CrossRef]
14. Yang, L.J.; Zeng, X.D.; Zhang, Y.M.; He, J.; Song, Z.L. Evolution of atmospheric corrosion of superplastic Zn-Al alloys exposed to an industrial environment. *Mater. Corros.* **2015**, *66*, 1169–1180. [CrossRef]
15. Vu, T.N.; Volovitch, P.; Ogle, K. The effect of pH on the selective dissolution of Zn and Al from Zn–Al coatings on steel. *Corros. Sci.* **2013**, *67*, 42–49. [CrossRef]
16. Xiao, L.; Liu, Q.; Wang, J.; Chen, N.; Chen, J.; Song, J.; Zhang, X.; Xiao, K. Study on corrosion mechanism of Al–Zn coatings in the simulated polluted marine atmosphere. *J. Mater. Res. Technol.* **2023**, *25*, 6446–6458. [CrossRef]

17. LeBozec, N.; Thierry, D.; Persson, D.; Stoulil, J. Atmospheric corrosion of zinc-aluminum alloyed coated steel in depleted carbon dioxide environments. *J. Electrochem. Soc.* **2018**, *165*, C343. [CrossRef]
18. *ISO 9227 NSS*; Corrosion Tests in Artificial Atmospheres—Salt Spray Tests (NSS, AASS, CASS). International Organization for Standardization: Geneva, Switzerland, 2017.
19. *ASTM B117*; Standard Practice for Operating Salt Spray (Fog) Apparatus. ASTM International: West Conshohocken, PA, USA, 2019.
20. Schürz, S.; Luckeneder, G.H.; Fleischanderl, M.; Mack, P.; Gsaller, H.; Kneissl, A.; Mori, G. Chemistry of corrosion products on Zn–Al–Mg alloy coated steel. *Corros. Sci.* **2010**, *52*, 3271–3279. [CrossRef]
21. Schmidt, D.; Shaw, B.; Sikora, E.; Shaw, W.; Laliberte, L. Comparison of testing techniques used to analyze the corrosion resistance of sacrificial coating systems. *Corrosion* **2007**, *63*, 958–974. [CrossRef]
22. DeForce, B.; Eden, T.J.; Pickering, H.W. Cold-sprayed aluminum coatings for magnesium aircraft components. *Mater. Perform.* **2009**, *48*, 40–44. [CrossRef]
23. Morcillo, M.; Palma, E.; Fernández, B. Atmospheric galvanic protection, of 55% Al-Zn precoated steel. *Mater. Corros.* **1994**, *45*, 550–553. [CrossRef]
24. Seré, P.; Zapponi, M.; Elsner, C.; Di Sarli, A. Comparative corrosion behaviour of 55Aluminium–zinc alloy and zinc hot-dip coatings deposited on low carbon steel substrates. *Corros. Sci.* **1998**, *40*, 1711–1723. [CrossRef]
25. Wallinder, I.O.; He, W.; Augustsson, P.; Leygraf, C. Characterization of black rust staining of unpassivated 55% Al–Zn alloy coatings. Effect of temperature, pH and wet storage. *Corros. Sci.* **1999**, *41*, 2229–2249. [CrossRef]
26. Hashemi, S.G.; Eghbali, B. Analysis of the formation conditions and characteristics of interphase and random vanadium precipitation in a low-carbon steel during isothermal heat treatment. *Int. J. Miner. Metall. Mater.* **2018**, *25*, 339–349. [CrossRef]
27. Deng, C.-M.; Xia, D.-H.; Zhang, R.; Behnamian, Y.; Hu, W.; Birbilis, N. On the localized corrosion of AA5083 in a simulated dynamic seawater/air interface—Part 2: Effects of wetting time. *Corros. Sci.* **2023**, *221*, 111367. [CrossRef]
28. Mansfeld, F. Tafel slopes and corrosion rates obtained in the pre-Tafel region of polarization curves. *Corros. Sci.* **2005**, *47*, 3178–3186. [CrossRef]
29. Wang, M.; Ji, Y.; Xia, D.-H.; Zhou, D.; Zhu, Y.; Gao, Z.; Qin, Z.; Hu, W. Effect of substrate orientations on the electrochemical and localized corrosion behavior of a quad-layer Al alloy composite. *J. Mater. Sci. Technol.* **2024**, *176*, 57–68. [CrossRef]
30. *ASTM G85*; Standard Practice for Modified Salt Spray (Fog) Testing. ASTM International: West Conshohocken, PA, USA, 2019.
31. *ISO 20340*; Paints and Varnishes—Performance Requirements for Protective Paint Systems for Offshore and Related Structures. International Organization for Standardization: Geneva, Switzerland, 2019.
32. *GB/T 16545-2015*; Corrosion of Metals and Alloys—Removal of Corrosion Products from Corrosion Test Specimens. Standardization Administration of China: Beijing, China, 2015.
33. Zhu, G.; Zhao, Y.; Liu, L.; Wang, L.; Wang, J.; Yu, S. Facile fabrication and evaluation of self-healing Zn-Al layered double hydroxide superhydrophobic coating on aluminum alloy. *J. Mater. Sci.* **2021**, *56*, 14803–14820. [CrossRef]
34. Cao, J.; Li, Y.; Chen, X.; Cai, D.; Zhou, S.-F.; Zhan, G. Preparation and multiple applications of integrated Zn-Al layered double hydroxide@polydopamine nanocomposites. *Mater. Today Commun.* **2022**, *31*, 103650. [CrossRef]
35. Ebrahimi, S.; Bordbar-Khiabani, A.; Yarmand, B. Immobilization of rGO/ZnO hybrid composites on the Zn substrate for enhanced photocatalytic activity and corrosion stability. *J. Alloys Compd.* **2020**, *845*, 156219. [CrossRef]
36. Deng, J.L. Introduction to grey system theory. *J. Grey Syst.* **1989**, *1*, 1–24.
37. Cao, X.; Deng, H.; Lan, W. Use of the grey relational analysis method to determine the important environmental factors that affect the atmospheric corrosion of Q235 carbon steel. *Anti-Corros. Methods Mater.* **2015**, *62*, 7–12. [CrossRef]
38. Fu, C.; Zheng, J.; Zhao, J.; Xu, W. Application of grey relational analysis for corrosion failure of oil tubes. *Corros. Sci.* **2001**, *43*, 881–889. [CrossRef]
39. Kuruvila, R.; Kumaran, S.T.; Khan, M.A. Optimization of erosion–corrosion behavior of nichrome coated 2205 duplex stainless steel using grey relational analysis. *Surf. Rev. Lett.* **2022**, *29*, 2250087. [CrossRef]

Disclaimer/Publisher's Note: The statements, opinions and data contained in all publications are solely those of the individual author(s) and contributor(s) and not of MDPI and/or the editor(s). MDPI and/or the editor(s) disclaim responsibility for any injury to people or property resulting from any ideas, methods, instructions or products referred to in the content.